

# Constraining turbulent heat flux parameterization over a temperate maritime glacier in New Zealand

J.P. CONWAY, N.J. CULLEN

*Department of Geography, University of Otago, Dunedin, New Zealand*  
*E-mail: jono.conway@otago.ac.nz*

**ABSTRACT.** The turbulent sensible and latent heat fluxes are important components of the surface energy balance over glaciers in the Southern Alps of New Zealand, contributing over half the energy available for ablation during large melt events. To calculate these terms confidently in glacier mass-balance models it is essential to use appropriate parameterizations for surface roughness and atmospheric stability. Eddy covariance measurements at Brewster Glacier were obtained over an ice surface to help facilitate an assessment of the calculation of the turbulent heat fluxes. The roughness length for momentum was found to be  $3.6 \times 10^{-3}$  m, while the roughness lengths for temperature and humidity were two orders of magnitude smaller, in agreement with surface renewal theory. A Monte Carlo approach was used to assess the uncertainty in turbulent heat fluxes calculated using the bulk aerodynamic method. It was found that input-data and roughness-length uncertainty could not explain underestimates of observed sensible heat fluxes during periods with low wind speed and large temperature gradients. During these periods a katabatic wind speed maximum alters the formulation of the turbulent exchange coefficient to that typically observed in a neutral atmosphere and this has implications for glacier mass-balance sensitivity.

## INTRODUCTION

To characterize the atmospheric controls on glacier mass balance and extract a climate signal from glaciers in the Southern Alps, New Zealand, a robust understanding of the surface energy balance (SEB) is needed. In the temperate maritime climate of the Southern Alps the turbulent sensible and latent heat fluxes are a key part of the SEB, contributing significantly to the energy available for ablation at the glacier surface. Point and distributed SEB studies show that turbulent heat fluxes provide ~50% of the melt energy during the ablation season (Anderson and others, 2010; Gillett and Cullen, 2011), while during large more infrequent melt events, turbulent heat fluxes dominate the energy balance, providing up to 80% of melt energy (Marcus and others, 1985; Hay and Fitzharris, 1988a). Thus, to assess the sensitivity of glacier mass balance to changes in atmospheric temperature and moisture, a robust estimation of turbulent heat fluxes is needed in energy- and mass-balance models.

Eddy covariance systems that directly measure turbulent heat fluxes are delicate and impractical for long-term studies, so energy- and mass-balance models often rely on the bulk aerodynamic method (bulk method) to calculate turbulent heat fluxes. According to Monin–Obukhov similarity theory, turbulence and turbulent heat fluxes above a surface can be related to gradients of wind speed, temperature and humidity (Monin and Obukhov, 1954). The well-constrained conditions at a glacier surface (zero wind speed and fully saturated surface) enable the bulk method to be driven with values of temperature, humidity and wind speed at a single height.

With high-quality in situ measurements of surface climate, the largest uncertainty in calculating turbulent heat fluxes using the bulk method comes from the roughness lengths of momentum ( $z_{0v}$ ), temperature ( $z_{0t}$ ) and humidity ( $z_{0q}$ ), which quantify the production of turbulence and transfer of heat and moisture towards or away from the surface. Values of  $z_{0v}$  derived over glacier ice surfaces vary

widely from  $3.0 \times 10^{-6}$  to  $1.2 \times 10^{-1}$  m (Bintanja and Van den Broeke, 1995; Van den Broeke, 1996). Previous estimates of  $z_{0v}$  over glacier ice surfaces in New Zealand have relied on profile methods, giving values of  $2.4 \times 10^{-3}$  and  $1.4 \times 10^{-2}$  m (Hay and Fitzharris, 1988b; Ishikawa and others, 1992). No estimates of  $z_{0t}$  or  $z_{0q}$  have been made and consequently all studies in New Zealand have assumed that  $z_{0v} = z_{0t} = z_{0q}$ . Owing to the large range of published values for  $z_0$ , many studies use an ‘effective’ roughness length  $z_{0\text{eff}}$  (where  $z_{0v} = z_{0t} = z_{0q}$ ) as a tuning variable to match modelled and observed ablation. Values obtained using this approach to characterize the surface energy and mass balance in the Southern Alps range from  $2.5 \times 10^{-3}$  to  $1.2 \times 10^{-2}$  m (Marcus and others, 1985; Anderson and others, 2010; Gillett and Cullen, 2011). The order-of-magnitude range in previously used values of  $z_{0\text{eff}}$  raises questions as to whether the magnitude of turbulent heat fluxes is being appropriately represented in the SEB compared with other terms controlling melt.

Turbulent heat flux parameterizations used within the bulk method in current glacier SEB models can be distinguished based on the treatment of atmospheric stability effects. Under conditions of flat homogeneous terrain, a stable atmosphere (increasing temperature with height) will resist the vertical movement of air and production of turbulence, thus reducing turbulent heat fluxes. Correspondingly, the vertical profiles of wind speed, temperature and humidity above the surface are altered, as are the relationships between turbulent heat fluxes and mean wind speed, temperature and humidity at a given level. The simplest form of parameterization used in the bulk method ignores atmospheric stability effects and assumes turbulent heat fluxes are related to logarithmic profiles of wind speed, temperature and humidity (Munro, 1991; Oerlemans, 2000; Machguth and others, 2006). Two methods are commonly used to account for atmospheric stability effects: the first through the bulk Richardson number ( $Ri_b$ ) (Wagon and

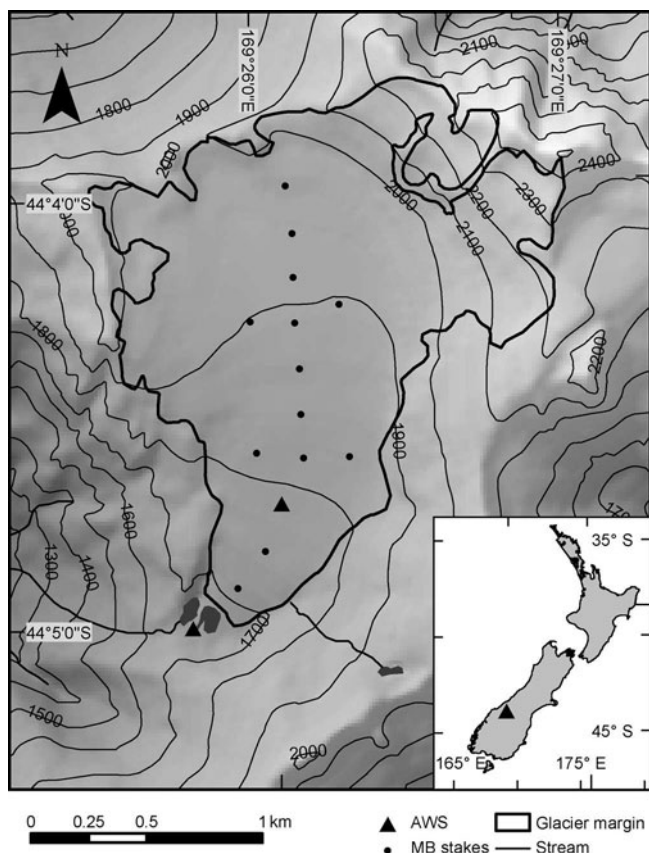


**Fig. 1.** Map of Brewster Glacier showing locations of AWS and surrounding topography. Contours are at 100 m intervals. Long-term mass-balance network (MB stakes) shown as filled circles.

others, 2003; Mölg and others, 2008; Anderson and others, 2010; Gillett and Cullen, 2011); the second through the Monin–Obukhov stability parameter ( $z/L$ ) (Braithwaite, 1995; Gerbaux and others, 2005 (after Brun and others, 1989); Klok and others, 2005; Van den Broeke and others, 2005; Dacic and others, 2008; Giesen and others, 2008; Hulth and others, 2010).

Stability functions based on these two metrics ( $Ri_b$  and  $z/L$ ) can have a large effect on calculated turbulent heat fluxes, especially over glacier surfaces where large positive temperature gradients often exist. Their effect becomes greatest during conditions of low wind speed ( $<3 \text{ m s}^{-1}$ ), with calculated turbulent heat fluxes rapidly approaching zero at critical stability thresholds at approximately 0.2 ( $Ri_b$ ) and 1 ( $z/L$ ). Unrealistic turbulent heat flux reduction can lead to underestimated melt and/or runaway cooling of surface temperatures, so many authors impose limits on stability functions during periods of low wind speed, such as: (1) removing stability functions for wind speed  $<1.5 \text{ m s}^{-1}$  (Gillett and Cullen, 2011); (2) setting a minimum value for wind speed (Brun and others, 1989; Martin and Lejeune, 1998); or (3) limiting the reduction in turbulent heat fluxes to 25–33% (Martin and Lejeune, 1998; Giesen and others, 2009).

It is essential to take into account uncertainty in glacier SEB models if robust estimates of turbulent heat fluxes are to be made. Monte Carlo simulations provide a useful method to assess the combined effects of input-variable and roughness-length uncertainty on modelled energy fluxes incorporating realistic physical feedbacks between elements of the SEB. Beyond uncertainty in automatic weather station (AWS)

measurements of surface layer wind speed, temperature and humidity, errors in the measured or simulated surface temperature can alter the magnitude of calculated turbulent heat fluxes by changing the lower boundary conditions of temperature and humidity used in the bulk method. Modelled surface and subsurface temperature depend on the excess or deficit of energy at the surface (Klok and Oerlemans, 2002; Mölg and others, 2008), so errors in other components of the energy balance, importantly the incoming radiative fluxes, can have a large impact on the calculated turbulent heat fluxes.

Given the important contribution turbulent heat fluxes make to the melt energy of temperate maritime glacier surfaces, it is imperative that uncertainties inherent in modelling these terms using the bulk method are addressed. With this in mind the current paper aims to use eddy covariance data to derive appropriate roughness lengths for momentum, temperature and humidity over a bare-ice glacier surface in New Zealand. In particular the paper focuses on the differences between the roughness length for momentum and those for the scalar fluxes of temperature and humidity. Turbulent heat fluxes observed using eddy covariance are compared with those modelled with the bulk method in Monte Carlo simulations that cover a range of turbulent heat flux and surface temperature schemes. This enables us to assess the treatment of atmospheric stability within the bulk method and its effect on modelled turbulent heat fluxes, while taking into account the effects of input-data and roughness-length uncertainty and different surface temperature parameterizations. A brief overview of the field site, data collection, Monte Carlo SEB simulations and eddy covariance data treatment is given before the results are presented and discussed.

## METHODS

The study uses data collected from Brewster Glacier, a small mountain glacier situated in the Southern Alps of New Zealand just to the west of the main divide (Fig. 1). Brewster Glacier has a southerly aspect, a surface area of  $2.5 \text{ km}^2$  and an elevation ranging from 1660 to 2400 m a.s.l. Data are utilized from two AWS: one on the central flowline of the glacier at 1760 m a.s.l. (AWS<sub>Glacier</sub>) and a second long-term station situated adjacent to the proglacial lake at 1650 m a.s.l. (AWS<sub>Lake</sub>). Mean annual air temperature at AWS<sub>Glacier</sub> was  $1.1^\circ\text{C}$  (October 2010–October 2011) and precipitation  $\sim 5 \text{ m w.e. a}^{-1}$ , split evenly between snow and rain. Summer (December–February) climate at AWS<sub>Glacier</sub> is characterized by moderately positive air temperatures (Table 1), an average wind speed of  $3.3 \text{ m s}^{-1}$  and an average vapour pressure in excess of that at the glacier surface (mean of  $7.2 \text{ hPa}$ ). The lower part of the glacier ( $<2000 \text{ m}$  and  $1.9 \text{ km}^2$  of its total area) is gently sloping ( $11^\circ$  mean slope), while the upper and smaller part of the glacier situated below the summit of Mount Brewster is steep ( $31^\circ$  mean slope) and contains a number of large ice cliffs. The glacier surface in the vicinity of AWS<sub>Glacier</sub> has an approximate mean gradient of  $6^\circ$ .

Data from AWS<sub>Glacier</sub> were used to force a surface energy- and mass-balance model (Mölg and others, 2008) that uses Eqn (1) to describe the SEB:

$$\text{SEB} = S_{\text{in}}(1 - \alpha) + L_{\text{in}} - \sigma \varepsilon T_0^4 + Q_S + Q_L + Q_R + Q_C \quad (1)$$

where  $S_{\text{in}}$  is the measured incoming solar radiation (corrected for slope angle; Van As, 2011),  $\alpha$  is the temporally

**Table 1.** Means and standard deviation (in parentheses) of climate (AWS<sub>Glacier</sub>) and turbulence data during the eddy covariance measurement period and long-term data from AWS<sub>Glacier</sub> during 2010/11. Roughness lengths are log mean values. Mean turbulent heat fluxes are obtained by the eddy covariance method using only stationary runs (168)

Parameter	Eddy covariance study period 8–16 February 2011	Summer 2010/11 (Dec–Feb)
Wind speed at 1.7 m (m s <sup>-1</sup> )	2.9 (1.4)	3.3
Air temperature at 1.3 m (°C)	4.5 (2.8)	4.7
Surface temperature (°C)	-0.7 (1.5)	-0.5
Vapour pressure at 1.3 m (hPa)	6.8 (1.7)	7.2
Atmospheric pressure (hPa)	826.0 (4.9)	820.0
Sensible heat flux ( $Q_S$ ) (W m <sup>-2</sup> )	39.3 (25.8)	
Latent heat flux ( $Q_L$ ) (W m <sup>-2</sup> )	0.83 (24.7)	
Stability ( $z/L$ )	0.35 (0.70)	
Roughness length for momentum ( $z_{0v}$ ) (m)	$3.6 \times 10^{-3}$ ( $2.8 \times 10^{-3}$ ) ( $n=37$ )	
Roughness length for temperature ( $z_{0t}$ ) (m)	$5.5 \times 10^{-5}$ ( $6.3 \times 10^{-5}$ ) ( $n=26$ )	
Roughness length for humidity ( $z_{0q}$ ) (m)	$1.2 \times 10^{-4}$ ( $3.2 \times 10^{-4}$ ) ( $n=20$ )	
Effective roughness length ( $z_{0\text{eff}}$ ) (m)	$6.3 \times 10^{-4}$ ( $2.7 \times 10^{-4}$ ) ( $n=26$ )	

averaged accumulated albedo (Van den Broeke and others, 2004),  $L_{\text{in}}$  is the measured incoming longwave radiation,  $\sigma$  is the Stefan–Boltzmann constant ( $5.87 \times 10^{-8} \text{ W m}^{-2}$ ),  $\varepsilon$  is the emissivity of snow/ice (equal to unity),  $T_0$  is the surface temperature (K),  $Q_S$  and  $Q_L$  are the turbulent sensible and latent heat fluxes, respectively,  $Q_R$  is the rain heat flux and  $Q_C$  is the conductive heat flux through the glacier sub-surface. Positive SEB values represent energy available for melting ( $Q_M$ ) while the SEB is equal to zero for  $T_0 < 273.15 \text{ K}$ . Energy fluxes directed towards the surface are treated as being positive. A number of different schemes to calculate  $T_0$  and  $Q_C$  were tested as were different parameterizations for  $Q_S$  and  $Q_L$ , with details of these provided later.  $Q_R$  was calculated from tipping-bucket rain gauge measurements at AWS<sub>Lake</sub>.

The bulk aerodynamic equations used to calculate  $Q_S$  and  $Q_L$  within the surface energy- and mass-balance model are:

$$Q_S = c_p \rho_0 \frac{p}{p_0} C U_z (T_z - T_0) \quad (2)$$

$$Q_L = 0.622 L_v \rho_0 \frac{1}{p_0} C U_z (e_z - e_0) \quad (3)$$

where  $c_p$  is the specific heat of air at constant pressure ( $1005 \text{ J kg}^{-1} \text{ K}^{-1}$ ),  $\rho_0$  is the density of air at standard sea level ( $1.29 \text{ kg m}^{-3}$  at  $0^\circ \text{C}$ ),  $L_v$  is the latent heat of vaporization ( $2.514 \text{ MJ kg}^{-1}$ ), replaced by the latent heat of sublimation ( $2.848 \text{ MJ kg}^{-1}$ ) if surface temperature ( $T_0$ ) is below the melting point,  $p$  is the actual air pressure (hPa),  $p_0$  is the air pressure at standard sea level (1013 hPa),  $C$  is a dimensionless exchange coefficient,  $U_z$ ,  $T_z$  and  $e_z$  are the wind speed ( $\text{m s}^{-1}$ ), air temperature (K) and vapour pressure (hPa) at height  $z$  (m), respectively, and  $e_0$  is the vapour pressure (hPa) at the surface. Four turbulent heat flux parameterizations used in current glacier SEB models were tested within the SEB model and are defined through the treatment of atmospheric stability effects on the exchange coefficient ( $C$ ). The first parameterization assumes that the turbulent heat fluxes are proportional to the neutral logarithmic profiles of wind speed and temperature with  $C$  given by:

$$C_{\log} = \frac{k^2}{\ln(z_v/z_{0v}) \ln(z_t/z_{0t})} \quad (4)$$

where  $k$  is the von Kármán constant (0.4),  $z_v$  and  $z_t$  are the

height of wind speed and temperature measurements, respectively, and  $z_{0v}$  and  $z_{0t}$  are the roughness lengths for momentum and temperature, respectively. Humidity measurements are made at  $z_t$  and it is assumed that  $z_{0q} = z_{0t}$ . The second parameterization includes a stability function based on the bulk Richardson number ( $Ri_b$ ) using the equation given by Monteith (1957), which leads to a flux reduction in stable conditions that is less than standard formulations (e.g. Wagon and others, 2003):

$$C_{Ri_b} = \frac{k^2}{\ln(z_v/z_{0v}) \ln(z_t/z_{0t})} (1 + 10 Ri_b)^{-1} \quad (5)$$

The third ( $C_{z/L}$ ) and fourth ( $C_{SR}$ ) parameterizations include an iterative stability function based on the Monin–Obukhov stability parameter  $z/L$ , where  $L$  is the Obukhov length scale (Van den Broeke and others, 2005):

$$C_{z/L} = \frac{k^2}{\left[ \ln\left(\frac{z_v}{z_{0v}}\right) - \psi_m\left(\frac{z_v}{L}\right) + \psi_m\left(\frac{z_{0v}}{L}\right) \right] \left[ \ln\left(\frac{z_t}{z_{0t}}\right) - \psi_h\left(\frac{z_t}{L}\right) + \psi_h\left(\frac{z_{0t}}{L}\right) \right]} \quad (6)$$

where  $\psi_m$  and  $\psi_h$  are the vertically integrated stability functions for momentum and heat, respectively. The expressions of Holtslag and de Bruin (1988) and Dyer (1974) are used to define  $\psi$  for stable and unstable conditions, respectively. The calculation of  $\psi$  requires an estimate of  $Q_S$ , so Eqs (2) and (6) are calculated iteratively. In all parameterizations both  $z_{0v}$  and  $z_{0t}$  ( $= z_{0q}$ ) were fixed to the log mean values obtained from eddy covariance measurements except for  $C_{SR}$ , where  $z_{0t}$  ( $= z_{0q}$ ) is defined by surface renewal theory using the expressions of Andreas (1987).

Eddy covariance measurements were made adjacent to AWS<sub>Glacier</sub> over a midsummer ice surface from 8 to 16 February 2011. Surface climate during the period was characterized by moderate wind speed and vapour pressure, with a mean air temperature of  $4.5^\circ \text{C}$  (Table 1). Eddy covariance instruments were mounted at 1.1 m with  $-0.2 \text{ m}$  surface height change during the study period. Three-dimensional (3-D) wind speed, sonic temperature (CSAT3, CSI) and vapour density (KH20, CSI) fluctuations were recorded at 20 Hz. The instruments were levelled to horizontal at daily intervals, with minimal change noted. Before calculating turbulence statistics, coordinate rotation was applied to the velocity data to align the streamlines into the

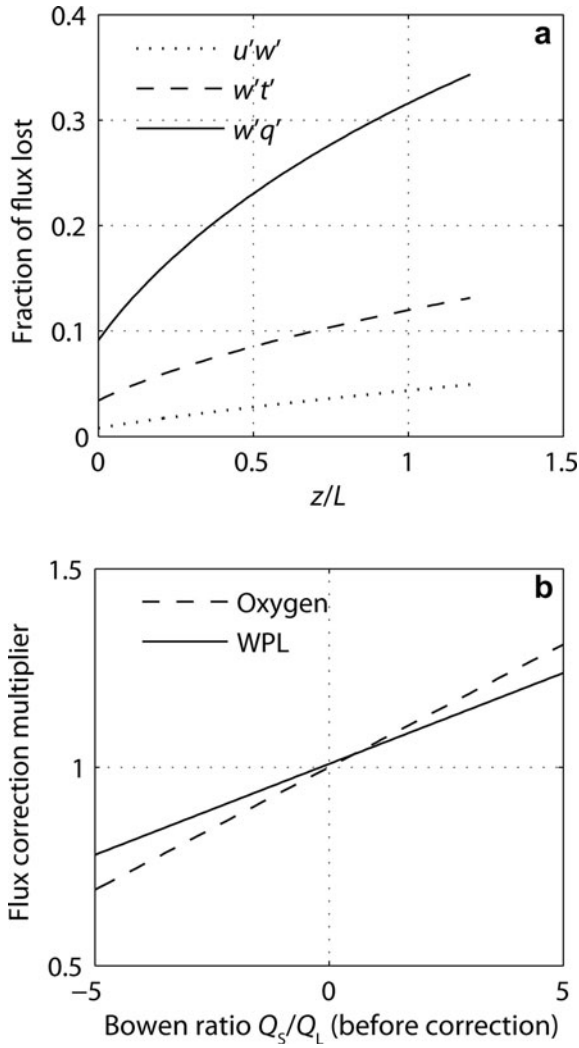


**Fig. 2.** Corrections to eddy covariance fluxes for (a) loss of high-frequency signal due to path-length averaging and sensor separation and (b) density and oxygen fluctuations in the path of the KH20 vapour density sensor.

mean flow for each 30 min run using a three-rotation scheme (Kaimal and Finnigan, 1994). Eddy covariance data were corrected for high-frequency flux loss due to the path-length averaging and separation of the CSAT3 and KH20 sensors (0.13 m), with average increases of 5–15% (Fig. 2a). Mean sonic temperature and sensible heat flux data were corrected for the effect of humidity fluctuations using the method of Schotanus and others (1983). The latent heat flux data were corrected for oxygen absorption by the KH20 (Tanner and others, 1993) and density effects using the ‘WPL’ correction (Webb and others, 1980), with corrections in the latent heat flux typically  $\pm 10\%$  (Fig. 2b). Larger corrections only occurred when absolute fluxes were small.

The covariances of the 3-D wind velocities ( $u$ ,  $v$ ,  $w$ ), temperature ( $T$ ) and vapour density ( $\rho_v$ ) were transferred to the friction velocity ( $u_*$ ), temperature scale ( $\theta_*$ ) and specific humidity scale ( $q_*$ ) using:

$$u_* = \left( \overline{u'w'^2} + \overline{v'w'^2} \right)^{0.25} \quad (7)$$

$$\theta_* = -\overline{w'T'}/u_* \quad (8)$$

$$q_* = -\overline{w'\rho_v'}/(u_*\rho_a) \quad (9)$$

where  $\rho_a$  is the air density at the mean temperature and pressure of  $\text{AWS}_{\text{Glacier}}$  ( $1.046 \text{ kg m}^{-3}$ ). These turbulent scales were then used to derive roughness lengths for each run of data using (e.g. Cullen and others, 2007):

$$z_{0v} = \exp \left[ -k \frac{U_z}{u_*} - \psi_m \left( \frac{z_v}{L} \right) \right] z_v \quad (10)$$

$$z_{0t} = \exp \left[ -k \frac{T_z - T_0}{\theta_*} - \psi_h \left( \frac{z_t}{L} \right) \right] z_t \quad (11)$$

$$z_{0q} = \exp \left[ -k \frac{q_z - q_0}{q_*} - \psi_h \left( \frac{z_t}{L} \right) \right] z_t \quad (12)$$

where  $U_z$  and  $T_z$  were determined using mean values of wind speed and temperature from the eddy covariance system, and specific humidity ( $q_{z,0}$ ) was calculated using  $T_{z,0}$  and relative humidity from  $\text{AWS}_{\text{Glacier}}$  (Buck, 1980), assuming the surface was at saturation (6.13 hPa). Vapour pressures were converted to specific humidity ( $\text{kg kg}^{-1}$ ) using  $q_{z,0} = 0.622 \times e_{z,0}/p$ .

A series of filters was applied to the 343 30 min runs obtained during the study period, to remove scatter and derive reliable roughness lengths. Data during precipitation events were removed, as these greatly increase measurement errors associated with the sonic anemometer. Wind direction was restricted to a  $60^\circ$  sector around the glacier fall line to minimize sensor arm interference and ensure the longest on-glacier fetch. Only stationary runs were used, following the method of Foken (2008). Again, the stability functions of Holtslag and de Bruin (1988) and Dyer (1974) were used to define  $\psi$  for stable and unstable conditions, respectively, but only runs with near-neutral conditions ( $-0.1 < z/L < 0.1$ ) were selected, so the choice of stability functions was not important. Runs were also selected for  $U_z > 3.0 \text{ m s}^{-1}$  and  $u_* > 0.1 \text{ m s}^{-1}$ , as errors in deriving  $z_{0v}$  become comparatively large as these values decrease, leaving a total of 37 runs. This small sample reflects the fact that situations of near-neutral stability on mid-latitude glaciers with katabatic forcing are fairly rare, as observed by Smeets and others (1998) who found only 55 half-hour periods that met the same conditions as above during the 2 month PASTEX (Pasterze experiment) campaign in Austria.

Another important consideration for deriving roughness lengths over glacier surfaces is to ensure that measurements are not affected by a low wind speed maximum. The difference in mean wind speed between the CSAT3 at 1.1 m and the RM Young anemometer at 1.7 m was used as a simple measure of wind shear in the vicinity of the eddy covariance measurements. During the conditions used to derive  $z_{0v}$ , wind speed was found to increase above the eddy covariance measurement height, so we are confident that the roughness lengths have been derived sufficiently below any wind speed maximum. Further analysis of the wind shear over a range of stabilities is described in the next section.

To determine  $z_{0t}$ , the gradient of temperature between the surface and the height of measurement must be well constrained. An uncertainty associated with the measured surface temperature of  $\pm 1^\circ \text{C}$  (Table 2) can cause an order-of-magnitude uncertainty in the calculated value of  $z_{0t}$ . To remove this uncertainty we selected data only when  $T_0 > -1^\circ \text{C}$  and  $T_z > 1^\circ \text{C}$  (to ensure sufficient temperature gradient) and assumed the glacier surface was melting during these conditions (Calanca, 2001). This resulted in a total of 26 runs to derive  $z_{0t}$ . To ensure a sufficient moisture gradient

to derive  $z_{0q}$ , a minimum vapour pressure gradient of  $|0.66|$  hPa was imposed, leaving 20 runs for the calculation of  $z_{0q}$ .

Monte Carlo simulations were made with the SEB model for the period of eddy covariance measurement (cf. Machguth and others, 2008) to assess the effect of input variable and roughness length uncertainty on turbulent heat fluxes calculated with the bulk method. A total of 40 000 simulations was conducted, with systematic and random errors being assigned to each input variable before each simulation and time-step, respectively. Errors were calculated by multiplying the uncertainties associated with each input variable (Table 2) by normally distributed random numbers ( $\mu=0$ ;  $\sigma=1$ ). Uncertainty in the derived value for  $z_{0v}$  was also included by calculating the roughness length at each time-step ( $i$ ) using:

$$z_{0v}(i) = 10^{\left[\log_{10}(z_{0v}) + \text{NORMRND}(\mu, \sigma)\right]} \quad (13)$$

where  $\text{NORMRND}(\mu, \sigma)$  is a MATLAB function that selects a random number from a normal distribution with a mean ( $\mu$ ) of 0 and standard deviation ( $\sigma$ ) of 0.274, which is the standard deviation of the 37 logarithmically transformed roughness length values. Four surface temperature schemes were used to calculate  $T_0$  and  $Q_C$ : (1) measured outgoing longwave radiation; (2) an iterative energy-balance closure scheme (Mölg and others, 2008); (3) a residual flux scheme in a surface layer of 0.2 m (Klok and Oerlemans, 2002); and (4) setting  $T_0$  at melting point for the entire period. At the start of each SEB simulation, one of the four turbulent heat flux parameterizations was randomly assigned in combination with one of the four surface temperature schemes. The modelled turbulent heat fluxes were then collated into the 16 resulting combinations before calculating means and standard deviations of  $Q_S$  and  $Q_L$  for each combination ( $n \sim 2500$ ) at each time-step. The resulting mean modelled turbulent heat fluxes were then compared with those observed with the eddy covariance instruments.

## RESULTS AND DISCUSSION

The roughness length for momentum ( $z_{0v}$ ) derived from eddy covariance was found to have a log mean value of  $3.6 \times 10^{-3}$  m (Table 1). This is similar to other values derived over mid-latitude glacier ice surfaces in the Southern Alps

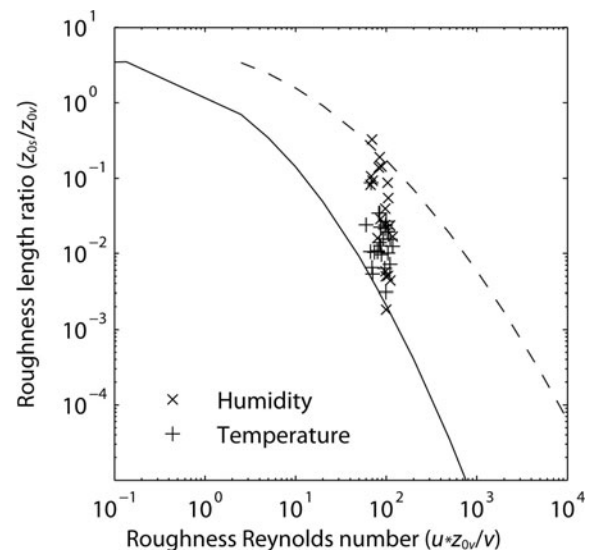


**Fig. 3.** The ratio of the roughness lengths for scalars ( $z_{0t}$  and  $z_{0q}$ ) and momentum ( $z_{0v}$ ) versus roughness Reynolds number ( $Re$ ). Also shown are the theoretical predictions of Andreas (1987) (solid line) and Smeets and Van den Broeke (2008) (dashed line). Points are individual 30 min runs and the log mean value of  $z_{0v}$  is used to calculate  $Re$ .

(Ishikawa and others, 1992) and the European Alps (Van den Broeke, 1997; Greuell and Smeets, 2001). More importantly, the roughness length for temperature ( $z_{0t}$ ) shows a log mean value of  $5.5 \times 10^{-3}$  m (Table 1), giving a ratio between the two roughness lengths ( $z_{0t}/z_{0v}$ ) of 0.015. That  $z_{0t}$  is several orders of magnitude smaller than  $z_{0v}$  compares well with surface renewal theory, with large roughness Reynolds numbers ( $Re = u_* z_{0v} / \nu$ ) indicating a rough flow regime. The measured ratios lie between the predictions of Andreas (1987) and those of Smeets and Van den Broeke (2008), derived for hummocky ice with  $z_{0v} > 1 \times 10^{-3}$  m (Fig. 3). The roughness length for humidity ( $z_{0q}$ ) was found to have a log mean value of  $1.2 \times 10^{-4}$  m (Table 1). This is slightly larger than  $z_{0t}$ , though the two values lie within one standard deviation of each other and the values are certainly within the measurement uncertainty associated with the determination of  $z_{0q}$ . Thus, our results do not support the idea that the roughness lengths for momentum and scalar fluxes can

**Table 2.** Variables measured and sensor specifications of AWS<sub>Glacier</sub> and eddy covariance instruments

Input variable	Instrument	Uncertainty
Wind speed ( $\text{m s}^{-1}$ )	RM Young 01503	$0.3 \text{ m s}^{-1}$
Air temperature ( $^{\circ}\text{C}$ )	Vaisala HMP 45AC	$0.2^{\circ}\text{C}$
Relative humidity (%)	Vaisala HMP 45AC	3%
Atmospheric pressure (hPa)	Vaisala PTB110	$0.5 \text{ hPa}$
Incoming shortwave radiation ( $\text{W m}^{-2}$ )	Kipp & Zonen CNR4	5%
Outgoing shortwave radiation ( $\text{W m}^{-2}$ )	Kipp & Zonen CNR4	5%
Incoming longwave radiation ( $\text{W m}^{-2}$ )	Kipp & Zonen CNR4	5%
Surface temperature ( $^{\circ}\text{C}$ )	Kipp & Zonen CNR4	$1^{\circ}\text{C}$
Precipitation (mm)*	TB4	25%
3-D wind speed ( $\text{m s}^{-1}$ )	CSI CSAT3 (ver.4)	$<0.04 \text{ m s}^{-1}$ ( $u_x$ and $u_y$ ); $<0.02 \text{ m s}^{-1}$ ( $u_z$ )
Sonic air temperature ( $^{\circ}\text{C}$ )	CSI CSAT3 (ver.4)	$0.025^{\circ}\text{C}^{\dagger}$
Vapour density ( $\text{g m}^{-3}$ )	CSI KH20	$<0.3 \text{ g m}^{-3}$

\*Uncertainty is estimated accounting for gauge undercatch.

$\dagger$ Measurement resolution of instrument.

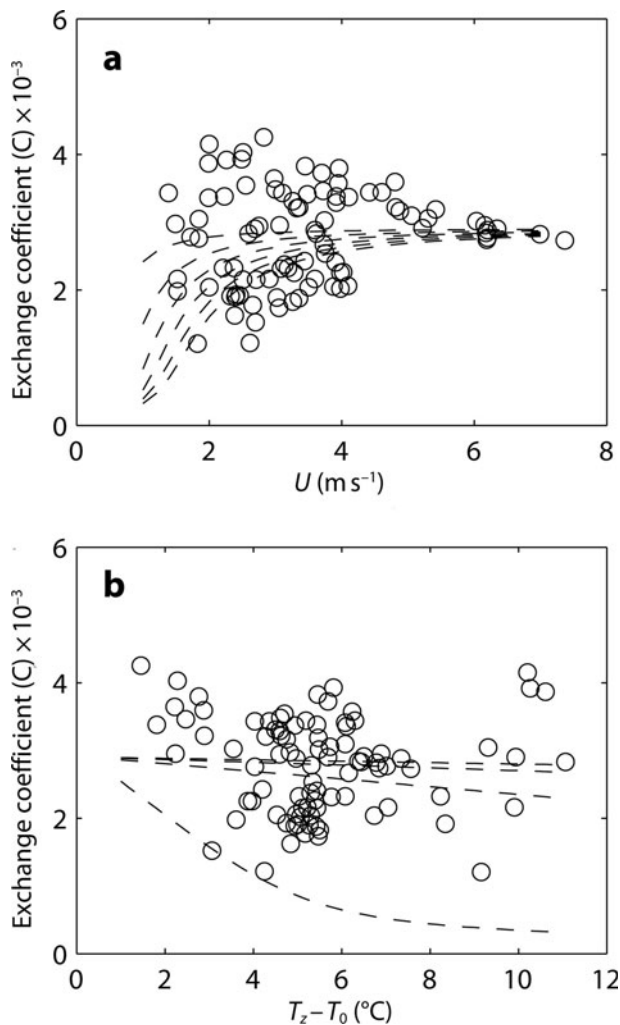


**Fig. 4.** Exchange coefficient ( $C_{\text{obs}}$ ) derived from eddy covariance measurements of the sensible heat flux against (a) wind speed and (b) temperature difference between air and surface. Shown as dashed lines are the exchange coefficients expected using the  $C_{z/L}$  parameterization (Eqn (6)).

be assumed equal, and find that  $z_{0t}$  and  $z_{0q}$  are approximately two orders of magnitude smaller than  $z_{0v}$  in an aerodynamically rough flow, as found over other mid-latitude glacier surfaces (Smeets and others, 1998). Our data do, however, support the use of equal roughness lengths for temperature and humidity.

To allow a comparison with ‘effective’ roughness lengths used previously in glacier SEB modelling, we derive a single ‘effective’ roughness length ( $z_{0\text{eff}}$ ) that assumes equality of the momentum and scalar roughness lengths, based on the same sample used to derive  $z_{0t}$ . The resulting log mean  $z_{0\text{eff}}$  is  $6.3 \times 10^{-4}$  m (Table 1), almost an order of magnitude smaller than those previously used in mass-balance modelling in the Southern Alps (Marcus and others, 1985; Hay and Fitzharris, 1988b). As  $z_{0t}$  is several orders of magnitude smaller than  $z_{0v}$  in an aerodynamically rough flow, the values of  $z_{0\text{eff}}$  are also at least an order of magnitude smaller than those for  $z_{0v}$ . Consequently, for scenarios in which only  $z_{0v}$  is derived over a glacier surface and the roughness lengths are assumed to be equal, the turbulent heat fluxes are likely to be overestimated. The potential to overestimate turbulent heat fluxes is large over temperate glaciers where a melting glacier surface presents no upper limit on  $z_{0\text{eff}}$

unless an independent check of modelled and observed surface temperature is made outside of melting conditions.

As roughness lengths can only be derived confidently in near-neutral conditions, we gain no information on the behaviour of the sensible heat flux in moderate or strongly stable conditions that dominate over the glacier surface. A first-order check can be made by examining the observed exchange coefficient ( $C_{\text{obs}}$ ) in more stable conditions. We derive  $C_{\text{obs}}$  using sensible heat flux ( $Q_{S\text{-eddy}}$ ),  $U_z$  and  $T_z$  from the eddy covariance instruments using Eqn (14), filtering the runs for precipitation, fetch and stationarity, as well as  $U_z > 1$  and  $T_z - T_0 > 1$  (90 runs):

$$C_{\text{obs}} = Q_{S\text{-eddy}} / \left( c_p \rho_0 \frac{P}{p_0} U_z (T_z - T_0) \right) \quad (14)$$

Figure 4 shows  $C_{\text{obs}}$  (black circles) against the observed wind speed (Fig. 4a) and temperature difference (Fig. 4b) for each 30 min run. Also shown is the expected value of  $C_{z/L}$  calculated using the bulk Eqns (2) and (6) across the same range of wind speed and temperature experienced during the study period (shown as dotted lines). As expected, more scatter in  $C_{\text{obs}}$  is found during low wind speeds and for smaller temperature differences, as measurement uncertainties become more important. A lower bound of points seems to follow the values predicted by Monin–Obukhov theory, perhaps indicating cases where a relatively high wind speed maximum allows Monin–Obukhov theory to hold. However, there is no overall trend toward decreasing  $C_{\text{obs}}$  for either a reduction in wind speed or an increase in temperature difference. Large values of  $C_{\text{obs}}$  occur during light and moderate wind speeds (1–4 m s<sup>-1</sup>) and a range of temperature differences. This implies that the magnitude of the sensible heat flux does not strictly follow Monin–Obukhov theory beyond near-neutral conditions.

We now compare turbulent heat fluxes measured using eddy covariance (observed) with those calculated using the bulk method within the SEB (modelled). Figure 5 presents the mean sensible heat flux ( $Q_S$ ) for each 30 min model time-step across the Monte Carlo simulations ( $n \sim 2500$ ) for combinations of four turbulent exchange coefficient ( $C$ ) parameterizations and four surface temperature schemes. Error bars show  $\pm 1$  standard deviation, and only time-steps with no precipitation and stationary eddy covariance data are shown (168 runs). The bulk method did not consistently replicate observed  $Q_S$ , with the performance of each parameterization within the bulk method associated with the treatment of atmospheric stability (Fig. 5). The  $C_{\text{log}}$  parameterization produced the best fit to observed  $Q_S$  across the full range of temperature and wind speed, with the lowest root-mean-square difference (rmsd  $11.2 \text{ W m}^{-2}$ ). Some of the larger-magnitude fluxes were slightly overestimated but remain mostly within the uncertainty introduced from the input data. The small bias ( $2.6\text{--}3.7 \text{ W m}^{-2}$ ) is encouraging as the use of the much simpler parameterization does not cause a large overestimate in the magnitude of  $Q_S$  as a whole. Parameterizations with stability functions ( $C_{\text{Rib}}$ ,  $C_{z/L}$ ,  $C_{\text{SR}}$ ) underestimate  $Q_S$ , independent of the surface temperature scheme used, showing biases of  $-4.1$  to  $-8.3 \text{ W m}^{-2}$ . The largest underestimates occurred during periods of light wind speed ( $< 3 \text{ m s}^{-1}$ ) and large positive gradients in temperature ( $> 2 \text{ K m}^{-1}$ ). During these conditions stability functions within the parameterizations dampened modelled  $Q_S$  close to zero while fluxes of  $50\text{--}100 \text{ W m}^{-2}$  were observed. A larger standard deviation in modelled  $Q_S$

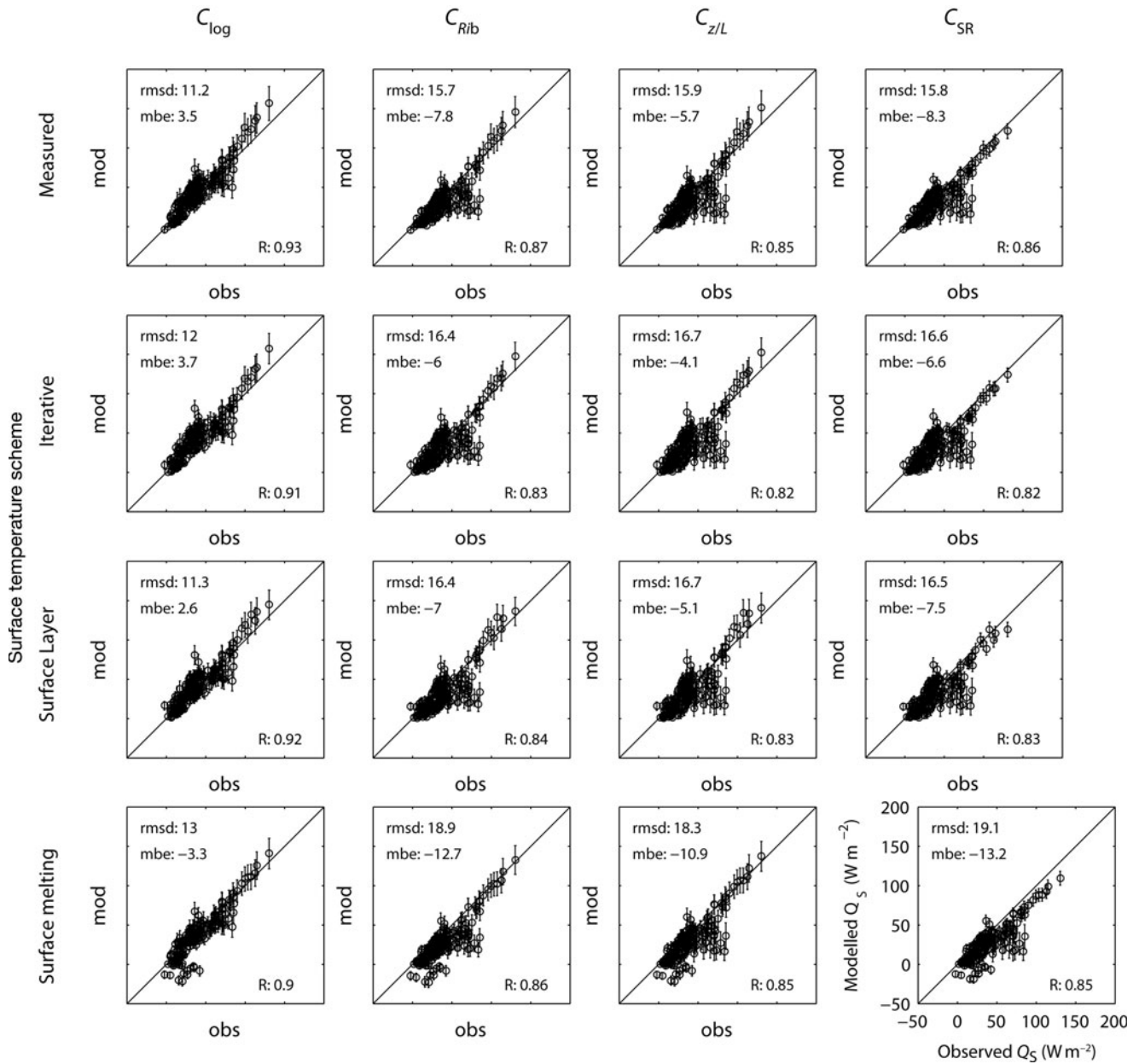


**Fig. 5.** Comparison of  $Q_s$  observed (CSAT3 eddy covariance system) and modelled (bulk method) for 16 combinations of sensible heat flux parameterization and surface temperature scheme. Dots and error bars show the mean and standard deviation of Monte Carlo ensembles with  $\sim 2500$  simulations per point. The bottom right axes gives the common scale in  $W m^{-2}$ . Root-mean-square difference (rmsd;  $W m^{-2}$ ), mean bias error (mbe;  $W m^{-2}$ ) and correlation coefficient ( $r$ ) are provided inside the axes for each combination.

is shown for these conditions, as uncertainties in input data become more important, but this uncertainty does not explain the underestimation.

The underestimation of  $Q_s$  during stable conditions is likely associated with the katabatic forcing of the glacier surface layer. Over sloping glacier surfaces, a positive temperature gradient creates negative buoyancy that drives the production of turbulence, rather than inhibiting turbulence as predicted by Monin–Obukhov theory (Oerlemans and Grisgono, 2002). In the katabatic flow, a wind speed maximum is formed, the height of which is proportional to the maximum wind speed of the flow and inversely related to surface slope (Denby and Greuell, 2000). Under conditions of low wind speed and over a steeply sloping surface, where the height of the wind speed maximum is typically lower, even a relatively low level of measurement ( $< 2$  m) is likely to be in the region of the wind speed

maximum. Figure 6 shows that for increasing atmospheric stability, as expressed through  $Ri_b$  and  $z/L$ , wind shear above the eddy covariance instruments is reduced with respect to near-neutral conditions. This indicates the presence of a wind speed maximum in the vicinity of the measurements for  $z/L > 0.1$ . In the region of the wind speed maximum, turbulent transport dominates the turbulent kinetic energy budget over vertical wind shear, and the momentum flux-profile relationship returns towards that of a neutral atmosphere (Denby and Smeets, 2000). Thus,  $Q_s$  calculated from our level of measurement ( $\sim 1.7$  m) is related to logarithmic profiles of wind speed and temperature in the presence of a wind speed maximum. Our data support this, showing that observed  $Q_s$  during conditions characterized by low wind speeds were best estimated using an exchange coefficient related to logarithmic wind speed and temperature profiles ( $C_{\log}$ ). A wind speed cut-off on the stability functions within

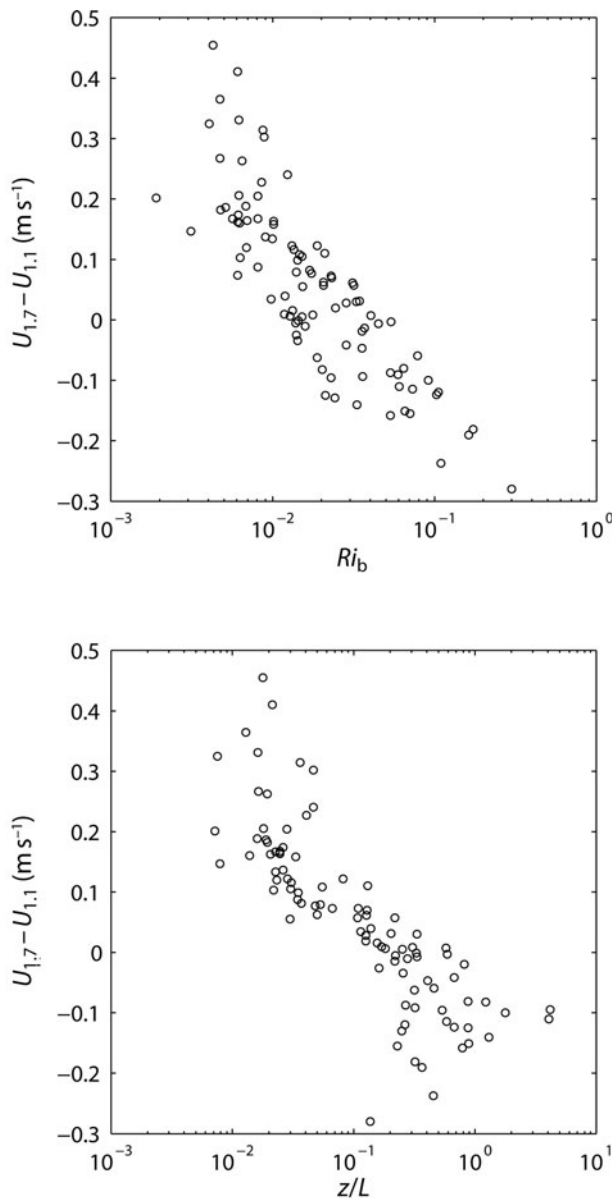


**Fig. 6.** Wind shear between CSAT3 measurement height (1.1 m) and RM Young measurement height (1.7 m) versus (a)  $Ri_b$  and (b)  $z/L$ .

$C_{Ri_b}$ ,  $C_{z/L}$  and  $C_{SR}$  only substantially improves the estimation of  $Q_S$  if the stability functions are removed for wind speeds  $< 3 \text{ m s}^{-1}$  (not shown), indicating that this may be the threshold at which the effect of the wind speed maximum becomes important at this site. This is near the threshold that stability functions also start to have a large effect on  $Q_S$  calculated using  $C_{Ri_b}$ ,  $C_{z/L}$  and  $C_{SR}$  within the bulk method.

The choice of turbulent heat flux parameterization becomes critically important when assessing the sensitivity of glacier mass balance to increasing ambient air temperatures, especially in a temperate maritime environment where the turbulent heat fluxes contribute a significant fraction of the melt energy at daily and seasonal timescales. For the  $C_{log}$  parameterization, the modelled sensitivity of  $Q_S$  depends only on the change in temperature gradient between the atmosphere and glacier surface. The use of parameterizations that include stability functions ( $C_{Ri_b}$ ,  $C_{z/L}$  and  $C_{SR}$ ) decreases the modelled sensitivity of melt energy to increased air temperature, as the stability functions decrease the exchange coefficient ( $C$ ) and counteract an increase in

temperature gradient in the calculation of  $Q_S$  (Eqn (2)) (cf. Braithwaite, 1995). In light wind conditions this can result in calculated  $Q_S$  decreasing as temperature increases. However, for glacier surfaces purely influenced by katabatic winds,  $Q_S$  is expected to increase quadratically with rising ambient temperature, as a result of a larger negative buoyancy force that amplifies the katabatic wind speed (Oerlemans and Grisgono, 2002). As the katabatic turbulent heat flux model is based on the temperature deficit between the glacier surface and ambient air, it requires observations of air temperature located away from the glacier surface and is not appropriate for use with in situ observations. The  $C_{log}$  parameterization, in contrast to parameterizations including stability functions, will always result in increased  $Q_S$  as air temperature increases, thus reproducing correctly the direction of feedback predicted by the katabatic model. This is especially important over glacier surfaces where large positive temperature gradients produce significant  $Q_S$  even during low wind-speed conditions. The  $C_{log}$  parameterization will also produce a more realistic assessment of  $Q_S$  when gradient winds rather than katabatic flows govern the profiles of wind speed above the glacier surface. Thus, for small mountain glaciers where in situ wind-speed and temperature data are available, the use of the  $C_{log}$  parameterization within the bulk method is recommended. An evaluation of the temperature sensitivity over longer timescales and across the full elevation range of the glacier would be needed to further explore the impact of this sensitivity on mass balance.

Modelled latent heat fluxes were unaffected by the choice of exchange coefficient parameterization, with very similar performance across the four parameterizations (not shown). Owing to the small vapour pressure gradient between surface and atmosphere during periods of high atmospheric stability within the study period, vapour fluxes are small during these periods and the effect of the stability correction term is not evident. To demonstrate this we show an example of modelled and observed latent heat fluxes for one set of exchange coefficient and surface temperature parameterizations (Fig. 7). The good agreement in both the magnitude and sign of observed  $Q_L$  (rmsd  $11.8 \text{ W m}^{-2}$ ) gives us confidence that  $Q_L$  can be reproduced using the bulk method using a roughness length for humidity equal to that for temperature.

The inclusion of a realistic surface temperature scheme was important in replicating observed  $Q_S$  and  $Q_L$ . Using the assumption of a melting surface, a negative bias in  $Q_S$  ( $-3.3$  to  $13.2 \text{ W m}^{-2}$ ) was produced, especially in those parameterizations using stability functions, and temporal changes in the sign of both  $Q_S$  and  $Q_L$  were not simulated correctly during periods of low (freezing) air temperatures (Figs 5 and 7). Surface temperature schemes that allowed for  $T_0 < 0^\circ\text{C}$  correctly simulated  $Q_S$  being directed towards the surface during periods of low (freezing) air temperature (Figs 5 and 8). Since both the iterative and residual layer surface temperature schemes replicated the temporal pattern of  $T_0$  well during each study period (Fig. 8), we gain further confidence that our model incorporates the main features of the glacier SEB in a physically realistic way. The inclusion of a realistic surface temperature scheme becomes especially important when investigating the magnitude of the turbulent heat fluxes and evolution of the SEB on daily timescales. The effect of disregarding conditions of non-melting  $T_0$  on the mass balance of continental glaciers has been shown by

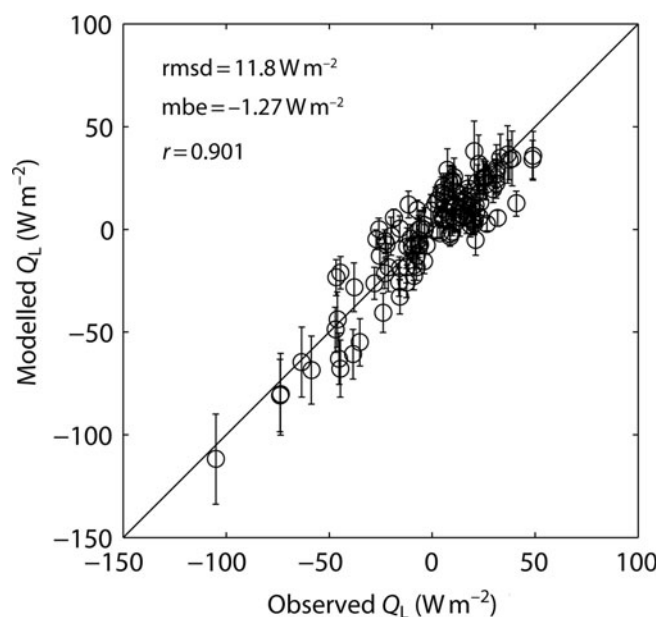


**Fig. 7.** Comparison of  $Q_L$  observed (CSAT3 eddy covariance system) and modelled (bulk method) during the ice period for the  $C_{log}$  parameterization. Surface temperature is calculated using the procedure described in Mölg and others (2008). Dots and error bars show the mean and standard deviation of Monte Carlo ensembles with 2618 simulations per point.

Pellicciotti and others (2009). However, further work is needed to constrain the surface and subsurface schemes used to model temperate maritime glacier mass balance to establish the effect of non-melting conditions in this environment. Importantly, the effect of refreezing meltwater and penetrating shortwave radiation on subsurface temperatures and mass balance needs further attention.

## CONCLUSIONS

We have addressed a number of uncertainties in calculating turbulent heat fluxes ( $Q_S$  and  $Q_L$ ) with the bulk method over a temperate maritime glacier. Eddy covariance measurements in near-neutral conditions showed a roughness length for momentum of  $3.6 \times 10^{-3}$  m over the glacier ice surface. Importantly, the scalar roughness lengths of temperature and humidity were found to be approximately two orders of magnitude smaller, in agreement with surface renewal theory. Vapour flux measurements supported the common assumption that the roughness lengths for temperature and humidity are equivalent. However, using the assumption that the scalar roughness lengths are equivalent to that for momentum in an aerodynamically rough flow will lead to overestimated turbulent heat fluxes when using the bulk method. With high-quality in situ measurements of wind speed, air temperature and relative humidity, observed turbulent sensible and latent heat fluxes can be reproduced with confidence using the bulk method, but only when an exchange coefficient based on logarithmic profiles of wind speed and temperature is used. Stability functions that reduce the exchange coefficient during positive temperature gradients are shown to underestimate the sensible heat flux under low wind-speed conditions, with Monte Carlo simulations showing that input-data and roughness-length uncertainty cannot account for this. This underestimation is likely due to the influence of a katabatically driven wind-speed maximum

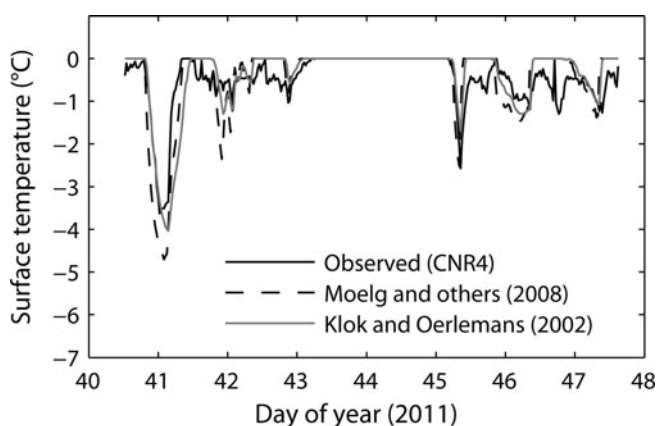


**Fig. 8.** Surface temperature during the study period showing measured surface temperature (black line) and that modelled using the expressions of Mölg and others (2008) (dashed line) and Klok and Oerlemans (2002) (grey line).

that, over moderately sloping glacier surfaces, exists near the level of AWS measurements and alters the turbulent exchange coefficient towards that typically observed in a neutral atmosphere. The choice of exchange coefficient has important implications when assessing the effect of rising ambient air temperatures on mountain glacier mass balance, as the temperature sensitivity of the turbulent heat fluxes is increased in environments that experience katabatic flows. In order to understand the mass-balance sensitivity in detail across the full range of elevations, further work is needed to constrain other components in the SEB. In particular, parameterizations to derive incoming longwave radiative fluxes from measurements of air temperature and humidity need to be evaluated further, as do the effects of non-melting conditions, refreezing meltwater and subsurface shortwave penetration on glacier mass balance.

## ACKNOWLEDGEMENTS

Funding from a University of Otago Research Grant (ORG10-10793101RAT) supported N. Cullen's contribution to this research. The research also benefited from the financial support of the National Institute of Water and Atmospheric Research, New Zealand (Climate Present and Past CLC01202), and collaboration with A. Mackintosh and B. Anderson, Victoria University of Wellington. We thank T. Mölg for input into the model, and P. Sirguey and W. Colgan for helpful discussions on the Monte Carlo approach. D. Howarth and N. McDonald provided careful technical support for the field measurements. We thank two anonymous reviewers and the scientific editor, T. Johanneson, for invaluable comments and suggestions that improved the manuscript.

## REFERENCES

- Anderson B and 6 others (2010) Climate sensitivity of a high-precipitation glacier in New Zealand. *J. Glaciol.*, **56**(195), 114–128 (doi: 10.3189/002214310791190929)
- Andreas EL (1987) A theory for the scalar roughness and the scalar transfer coefficients over snow and sea ice. *Bound.-Layer Meteorol.*, **38**(1–2), 159–184 (doi: 10.1007/BF00121562)
- Bintanja R and Van den Broeke MR (1995) Momentum and scalar transfer coefficients over aerodynamically smooth Antarctic

- surfaces. *Bound.-Layer Meteorol.*, **74**(1–2), 89–111 (doi: 10.1007/BF00715712)
- Braithwaite RJ (1995) Aerodynamic stability and turbulent sensible heat flux over a melting ice surface, the Greenland ice sheet. *J. Glaciol.*, **41**(139), 562–571
- Brun E, Martin E, Simon V, Gendre C and Coléou C (1989) An energy and mass model of snow cover suitable for operational avalanche forecasting. *J. Glaciol.*, **35**(121), 333–342
- Buck AL (1981) New equations for computing vapor pressure and enhancement factor. *J. Appl. Meteorol.*, **20**(12), 1527–1532 (doi: 10.1175/1520-0450(1981)020<1527:NEFCVP>)
- Calanca P (2001) A note on the roughness length for temperature over melting snow and ice. *Q. J. R. Meteorol. Soc.*, **127**(571), 255–260 (doi: 10.1002/qj.49712757114)
- Cullen NJ, Mölg T, Kaser G, Steffen K and Hardy DR (2007) Energy balance model validation on the top of Kilimanjaro, Tanzania, using eddy covariance data. *Ann. Glaciol.*, **46**, 227–233 (doi: 10.3189/172756407782871224)
- Dadic R, Corripio JG and Burlando P (2008) Mass-balance estimates for Haut Glacier d'Arolla, Switzerland, from 2000 to 2006 using DEMs and distributed mass-balance modeling. *Ann. Glaciol.*, **49**, 22–26 (doi: 10.3189/172756408787814816)
- Denby B and Greuell W (2000) The use of bulk and profile methods for determining surface heat fluxes in the presence of glacier winds. *J. Glaciol.*, **46**(154), 445–452 (doi: 10.3189/172756500781833124)
- Denby B and Smeets P (2000) Derivation of turbulent flux profiles and roughness lengths from katabatic flow dynamics. *J. Appl. Meteorol.*, **39**(9), 1601–1612 (doi: 10.1175/1520-0450(2000)039.1601)
- Dyer AJ (1974) A review of flux-profile relationships. *Bound.-Layer Meteorol.*, **7**(3), 363–372 (doi: 10.1007/BF00240838)
- Foken T (2008) *Micrometeorology*. Springer, Berlin
- Gerbaux M, Genthon C, Etchevers P, Vincent C and Dedieu JP (2005) Surface mass balance of glaciers in the French Alps: distributed modeling and sensitivity to climate change. *J. Glaciol.*, **51**(175), 561–572 (doi: 10.3189/172756505781829133)
- Giesen RH, Van den Broeke MR, Oerlemans J and Andreassen LM (2008) Surface energy balance in the ablation zone of Midtdalsbreen, a glacier in southern Norway: interannual variability and the effect of clouds. *J. Geophys. Res.*, **113**(D21), D21111 (doi: 10.1029/2008JD010390)
- Giesen RH, Andreassen LM, Van den Broeke MR and Oerlemans J (2009) Comparison of the meteorology and surface energy balance at Storbreen and Midtdalsbreen, two glaciers in southern Norway. *Cryosphere*, **3**(1), 57–74
- Gillett S and Cullen NJ (2011) Atmospheric controls on summer ablation over Brewster Glacier, New Zealand. *Int. J. Climatol.*, **31**(13), 2033–2048 (doi: 10.1002/joc.2216)
- Greuell W and Smeets P (2001) Variations with elevation in the surface energy balance on the Pasterze (Austria). *J. Geophys. Res.*, **106**(D23), 31 717–31 727 (doi: 10.1029/2001JD900127)
- Hay JE and Fitzharris BB (1988a) The synoptic climatology of ablation on a New Zealand glacier. *Int. J. Climatol.*, **8**(2), 201–215 (doi: 10.1002/joc.3370080207)
- Hay JE and Fitzharris BB (1988b) A comparison of the energy-balance and bulk-aerodynamic approaches for estimating glacier melt. *J. Glaciol.*, **34**(117), 145–153
- Holtslag AAM and de Bruin HAR (1988) Applied modeling of the nighttime surface energy balance over land. *J. Appl. Meteorol.*, **27**(6), 689–704 (doi: 10.1175/1520-0450(1988)027<0689:AMOTNS>2.0.CO;2)
- Hulth J, Rolstad C, Trondsen K and Wedøe Rødby R (2010) Surface mass and energy balance of Sørbreen, Jan Mayen, 2008. *Ann. Glaciol.*, **51**(55), 110–119 (doi: 10.3189/172756410791392754)
- Ishikawa N, Owens IF and Sturman AP (1992) Heat balance characteristics during fine periods on the lower part of the Franz Josef Glacier, South Westland, New Zealand. *Int. J. Climatol.*, **12**(4), 397–410 (doi: 10.1002/joc.3370120407)
- Kaimal JC and Finnigan JJ (1994) *Atmospheric boundary layer flows: their structure and measurement*. Oxford University Press, Oxford
- Klok EJ and Oerlemans J (2002) Model study of the spatial distribution of the energy and mass balance of Morteratschgletscher, Switzerland. *J. Glaciol.*, **48**(163), 505–518 (doi: 10.3189/172756502781831133)
- Klok EJ, Nolan M and Van den Broeke MR (2005) Analysis of meteorological data and the surface energy balance of McCall Glacier, Alaska, USA. *J. Glaciol.*, **51**(174), 451–461 (doi: 10.3189/172756505781829241)
- Machguth H, Paul F, Hoelzle M and Haeberli W (2006) Distributed glacier mass-balance modelling as an important component of modern multi-level glacier monitoring. *Ann. Glaciol.*, **43**, 335–343 (doi: 10.3189/172756406781812285)
- Machguth H, Purves RS, Oerlemans J, Hoelzle M and Paul F (2008) Exploring uncertainty in glacier mass-balance modelling with Monte Carlo simulation. *Cryosphere*, **2**(2), 191–204 (doi: 10.5194/tc-2-191-2008)
- Marcus MG, Moore RD and Owens IF (1985) Short-term estimates of surface energy transfers and ablation on the lower Franz Josef Glacier, South Westland, New Zealand. *New Zeal. J. Geol. Geophys.*, **28**(3), 559–567 (doi: 10.1080/00288306.1985.10421208)
- Martin E and Lejeune Y (1998) Turbulent fluxes above the snow surface. *Ann. Glaciol.*, **26**, 179–183
- Mölg T, Cullen NJ, Hardy DR, Kaser G and Klok L (2008) Mass balance of a slope glacier on Kilimanjaro and its sensitivity to climate. *Int. J. Climatol.*, **28**, 881–892 (doi: 10.1002/joc.1589)
- Monin AS and Obukhov AM (1954) Osnovnie haraktristiki turbulentnogo peremeshivaniya v prizemnom sloe atmosferi [Main characteristics of turbulent mixing in atmospheric boundary layer]. *Trudy Inst. Geofiz. (Akad. Nauk SSSR)*, **24**, 163–187
- Monteith JL (1957) Dew. *Q. J. R. Meteorol. Soc.* **83**(357), 322–341 (doi: 10.1002/qj.49708335706)
- Munro DS (1991) A surface energy exchange model of glacier melt and net mass balance. *Int. J. Climatol.*, **11**(6), 689–700
- Oerlemans J (2000) Analysis of a 3 year meteorological record from the ablation zone of Morteratschgletscher, Switzerland: energy and mass balance. *J. Glaciol.*, **46**(155), 571–579 (doi: 10.3189/172756500781832657)
- Oerlemans J and Grisogono B (2002) Glacier winds and parameterization of the related surface heat fluxes. *Tellus*, **54A**(5), 440–452
- Pellicciotti F, Carenzo M, Helbing J, Rimkus S and Burlando P (2009) On the role of the subsurface heat conduction in glacier energy-balance modelling. *Ann. Glaciol.*, **50**(50), 16–24 (doi: 10.3189/172756409787769555)
- Schotanus P, Nieuwstadt FTM and Bruin HAR (1983) Temperature measurement with a sonic anemometer and its application to heat and moisture fluxes. *Bound.-Layer Meteorol.*, **26**(1), 81–93 (doi: 10.1007/BF00164332)
- Smeets CJPP and Van den Broeke MR (2008) The parameterization of scalar transfer over rough ice. *Bound.-Layer Meteorol.*, **128**(3), 339–355 (doi: 10.1007/s10546-008-9292-z)
- Smeets CJPP, Duykerke PG and Vugts HF (1998) Turbulence characteristics of the stable boundary layer over a mid-latitude glacier. Part 1: A combination of katabatic and large-scale forcing. *Bound.-Layer Meteorol.*, **87**(1), 117–145 (doi: 10.1023/A:1000860406093)
- Tanner BD, Swiatek E and Greene JP (1993) Density fluctuations and use of the krypton hygrometer in surface flux measurements. In *Proceedings of the 1993 National Conference on Irrigation and Drainage Engineering, Irrigation and Drainage Division, 21–23 July 1993, Park City, UT*. American Society of Civil Engineers, New York, 945–952 (ASCE Technical Note 4-93MP)
- Van As D (2011) Warming, glacier melt and surface energy budget from weather station observations in the Melville Bay region of northwest Greenland. *J. Glaciol.*, **57**(202), 208–220 (doi: 10.3189/002214311796405898)

- Van den Broeke M (1996) Characteristics of the lower ablation zone of the West Greenland ice sheet for energy-balance modelling. *Ann. Glaciol.*, **23**, 160–166
- Van den Broeke MR (1997) Momentum, heat and moisture budgets of the katabatic wind layer over a large mid-latitude glacier in summer. *J. Appl. Meteorol.*, **36**(6), 763–774 (doi: 10.1175/1520-0450(1997)036<0763:MHAMBO>2.0.CO;2)
- Van den Broeke MR, Van As D, Reijmer C and Van de Wal R (2004) Assessing and improving the quality of unattended radiation observations in Antarctica. *J. Atmos. Oceanic Technol.*, **21**(9), 1417–1431
- Van den Broeke MR, Van As D, Reijmer C and Van de Wal R (2005) Sensible heat exchange at the Antarctic snow surface: a study with automatic weather stations. *Int. J. Climatol.*, **25**(8), 1081–1101 (doi: 10.1002/joc.1152)
- Wagnon P, Sicart JE, Berthier E and Chazarin JP (2003) Wintertime high-altitude surface energy balance of a Bolivian glacier, Illimani, 6340 m above sea level. *J. Geophys. Res.*, **108**(D6), 4177 (doi: 10.1029/2002JD002088)
- Webb EK, Pearman GI and Leuning R (1980) Correction of flux measurements for density effects due to heat and water vapour transfer. *Q. J. R. Meteorol. Soc.*, **106**(447), 85–100 (doi: 10.1002/qj.49710644707)